Supporting information for

High–Throughput Screening Permeability Separator with High Catalytic Conversion Kinetics for Li–S Batteries

Yuting Jiang [a], Pei Liang [b], Mingjian Tang [c], Shipeng Sun [c], Huihua Min [d], Jiachen Han [a], Xiaodong Shen [a], Hao Yang *[a], Dongliang Chao [e], Jin Wang *[a]

[a] College of Materials Science and Engineering, Nanjing Tech University, Nanjing 211800, PR China

E–mail: msejwang@njtech.edu.cn (J. Wang); mse_yanghao@njtech.edu.cn

[b] College of Optical and Electronic Technology, China Jiliang University, Hangzhou 310018, PR China

[c] State Key Laboratory of Materials–Oriented Chemical Engineering, Jiangsu National Synergetic Innovation Center for Advanced Materials, College of Chemical Engineering, Nanjing Tech University, Nanjing 211816, China

[d] Electron Microscope Lab, Nanjing Forestry University, Nanjing 210037, Jiangsu, PR China

[e] Laboratory of Advanced Materials, Shanghai Key Laboratory of Molecular Catalysis and Innovative Materials, State Key Laboratory of Molecular Engineering of Polymers, and School of Chemistry and Materials, Fudan University, Shanghai, 200433, China.

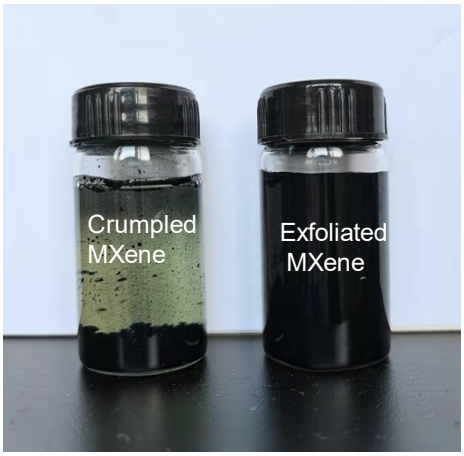

Figure S1 The digital photo of exfoliated few-layered MXene solution and crumpled MXene flocculation.

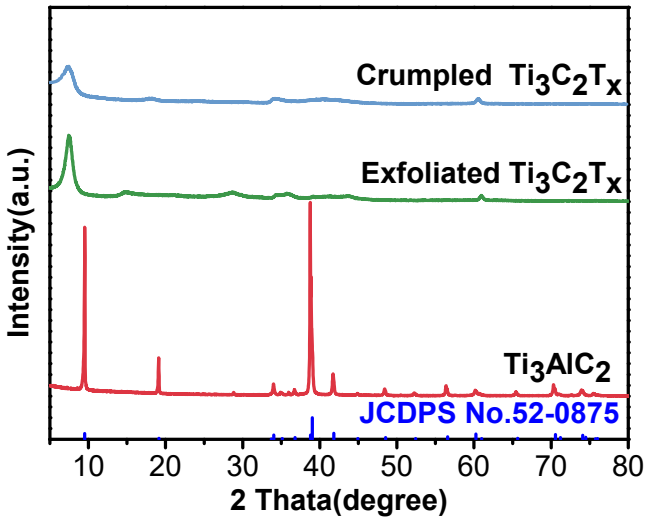

Figure S2 XRD patterns of Ti_3AlC_2, $Ti_3C_2T_x$ and crumpled $Ti_3C_2T_x$ nanosheets.

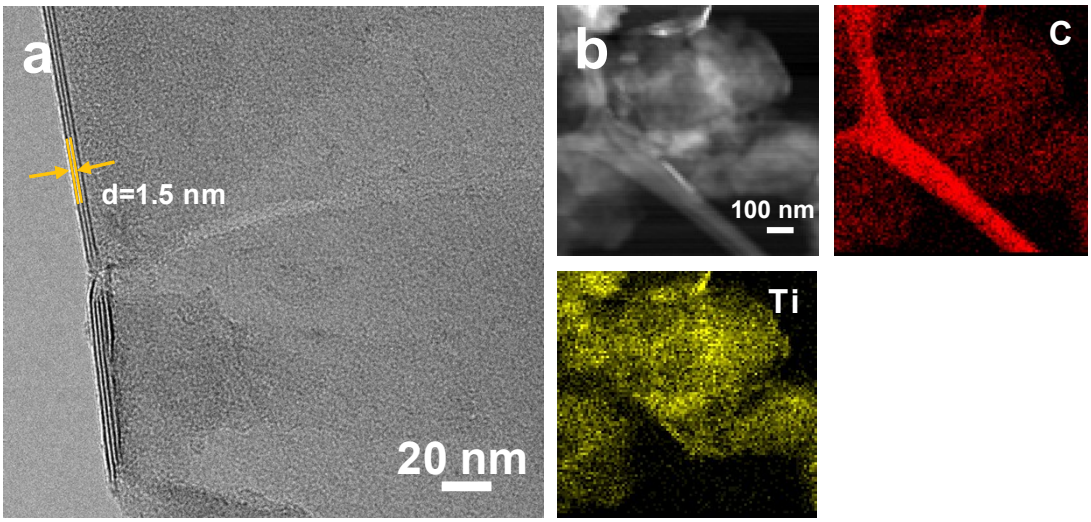

Figure S3 (a) TEM image of delaminated MXene nanosheets showing an interlayer spacing of 1.5 nm. (b) HAADF–STEM image and the corresponding elemental mapping images of delaminated MXene.

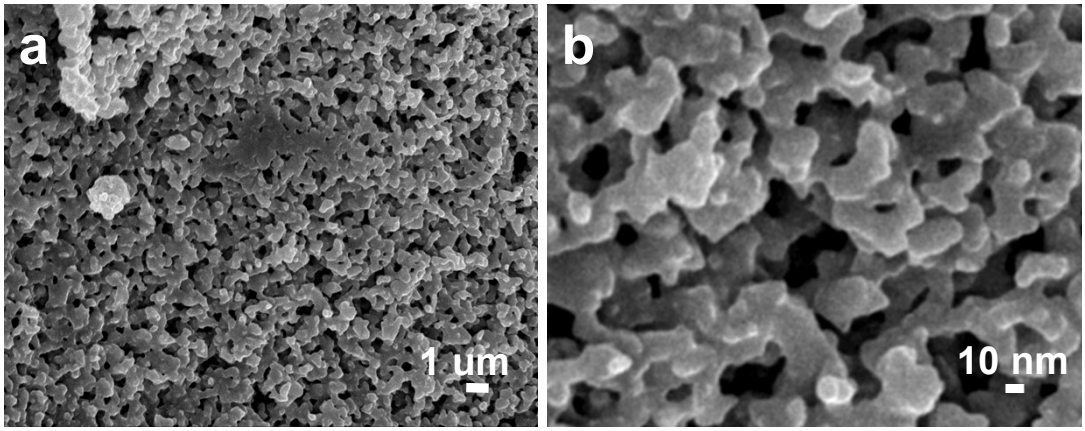

Figure S4 SEM images of MoS_2 prepared without crumpled MXene.

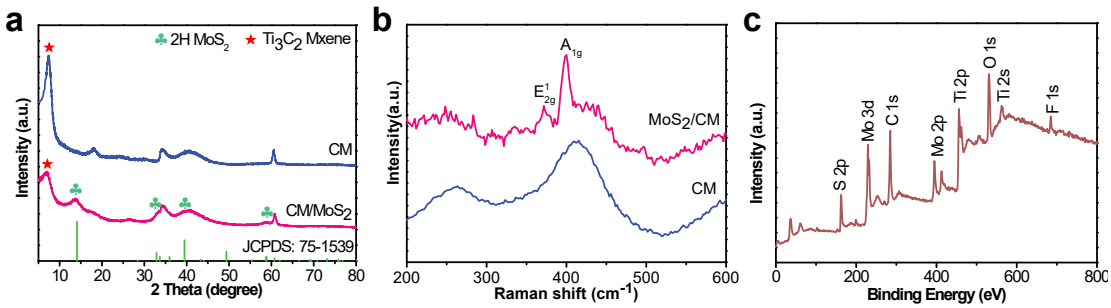

Figure S5 (a) XRD patterns of CM and CM/MoS_2. (b) Raman patterns of CM and CM/MoS_2. (c) XPS survey spectra of CM/MoS_2.

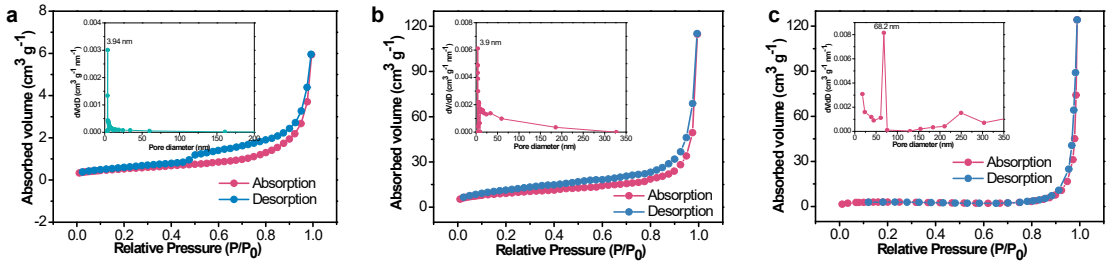

Figure S6 N_2 adsorption/desorption isotherms and the corresponding pore size distribution of (a) CM/MoS2, (b) MoS_2 and (c) CM.

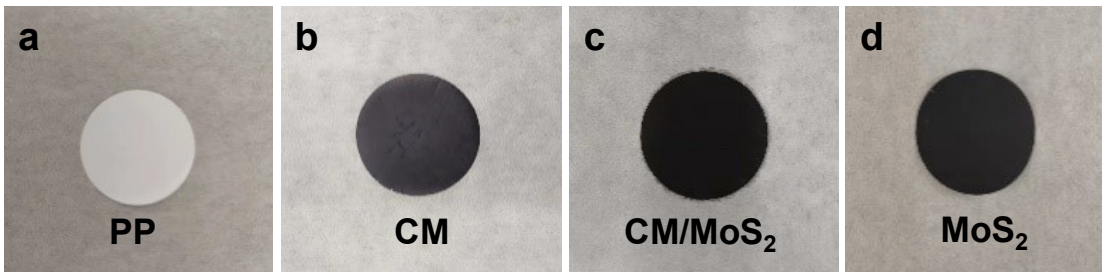

Figure S7 The digital photographs of the fabricated functional separators displaying distinguishable color compared with the pristine PP separator.

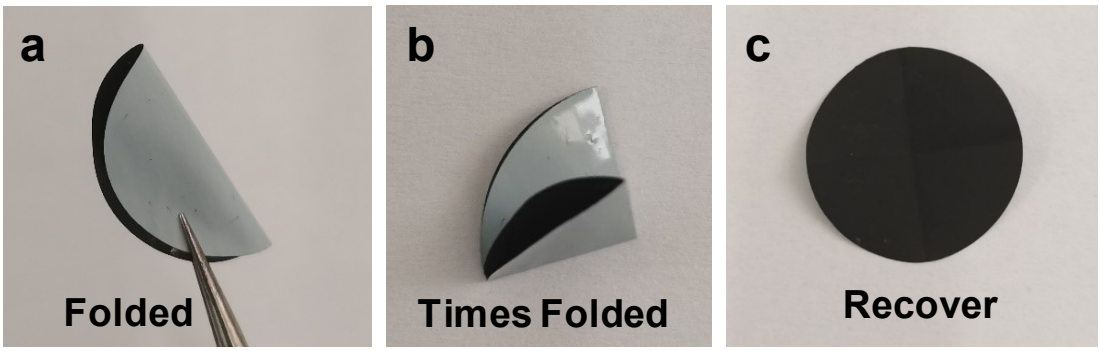

Figure S8 The digital photo of (a) folded, (b) several times folded and (c) recovered CM/MoS_2 separators.

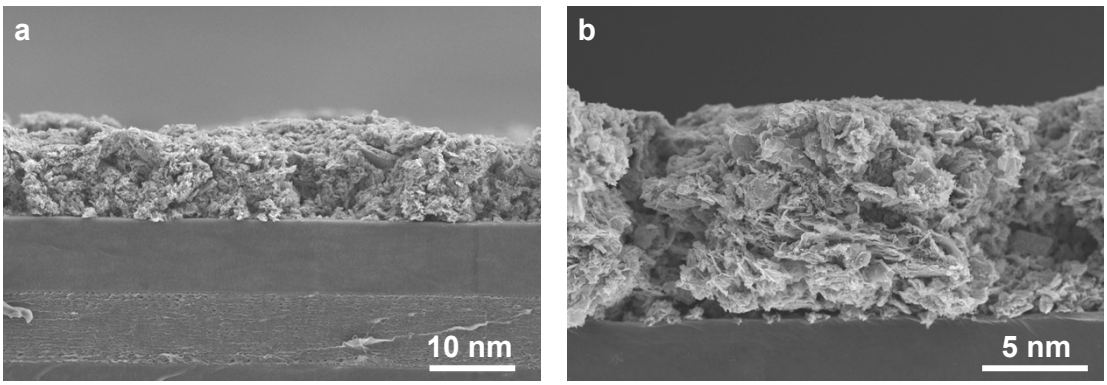

Figure S9 Cross–section SEM images of CM/MoS_2–modified PP separator.

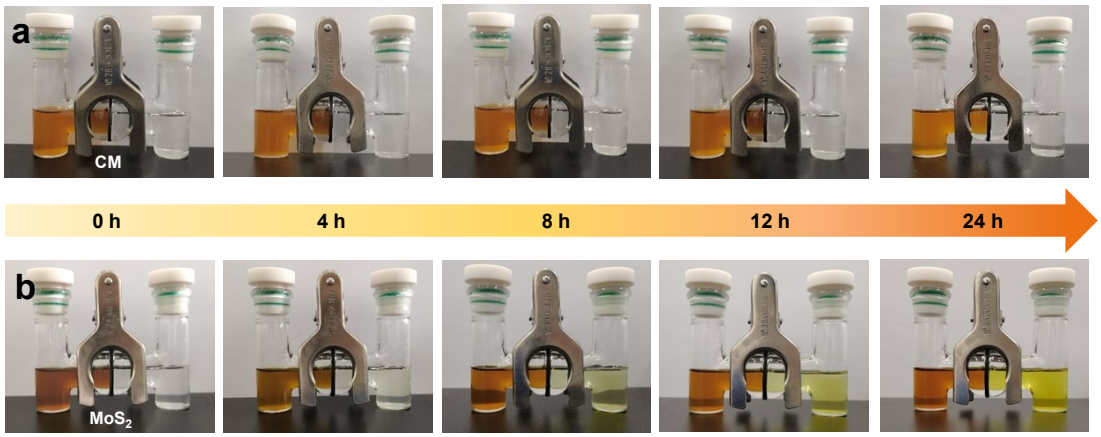

Figure S10 Polysulfides permeation measurements with H-shaped glass cells using (a) CM-modified separator and (b) MoS_2-modified separator.

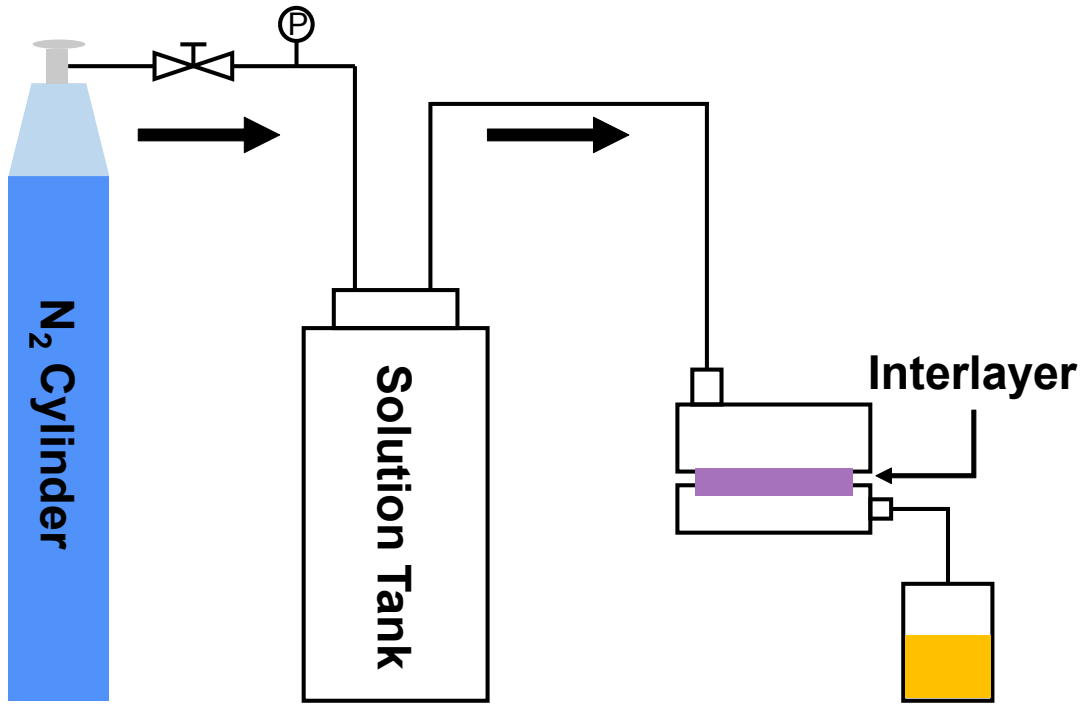

Figure S11 The schematic dead–end filtration system for the measurement of electrolyte permeability in various separators.

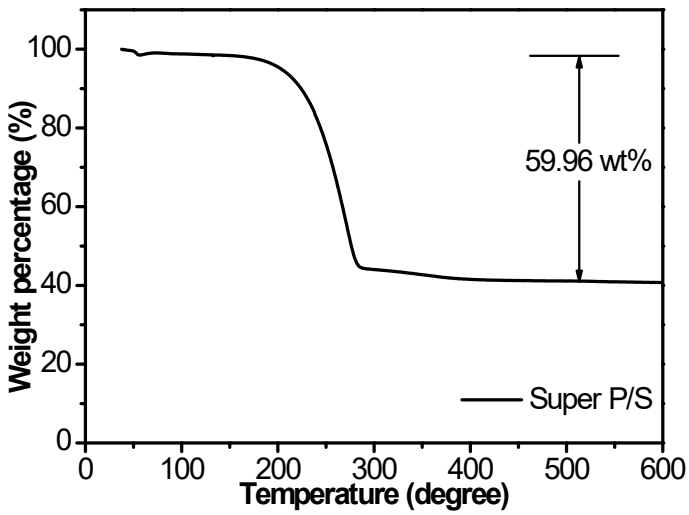

Figure S12 TGA curve of a Super P Black/S cathode.

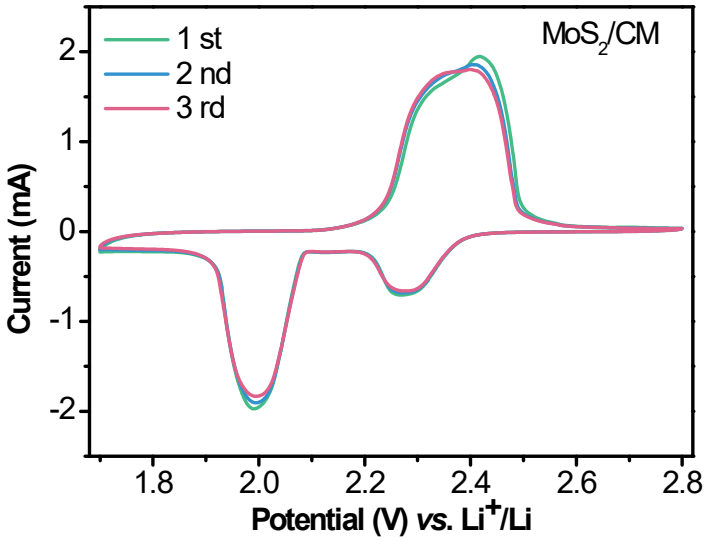

Figure S13 Cyclic voltammetry curves of the Li-S battery with CM/MoS_2 separator in the first three cycles.

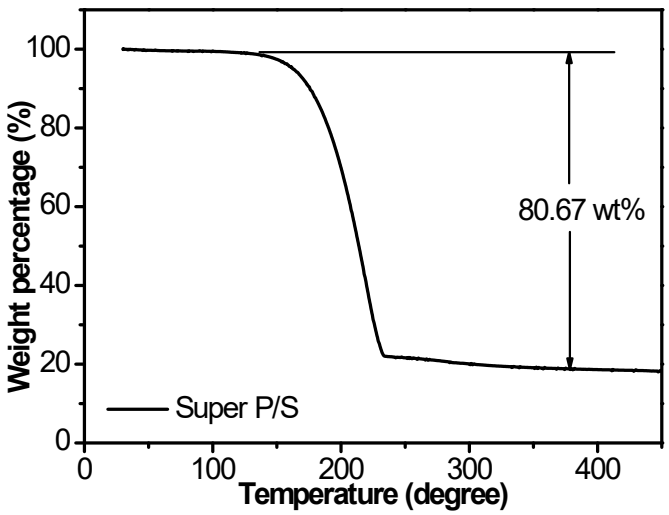

Figure S14 TGA curve of a Super P/S cathode with a high sulfur loading of 5 mg cm^{-2} with a sulfur content of 80%.

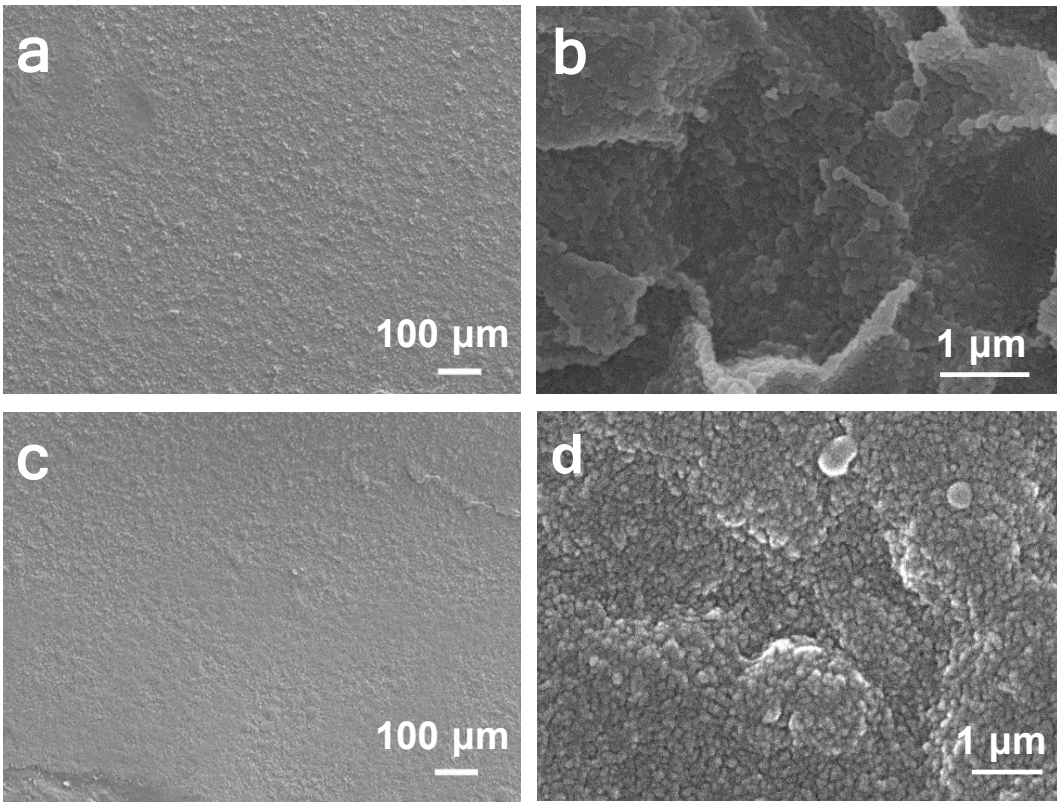

Figure S15 SEM images of the CM/MoS_2 modified separator adjacent to the cathode side (a-b) before and (c-d) after 100 cycles.

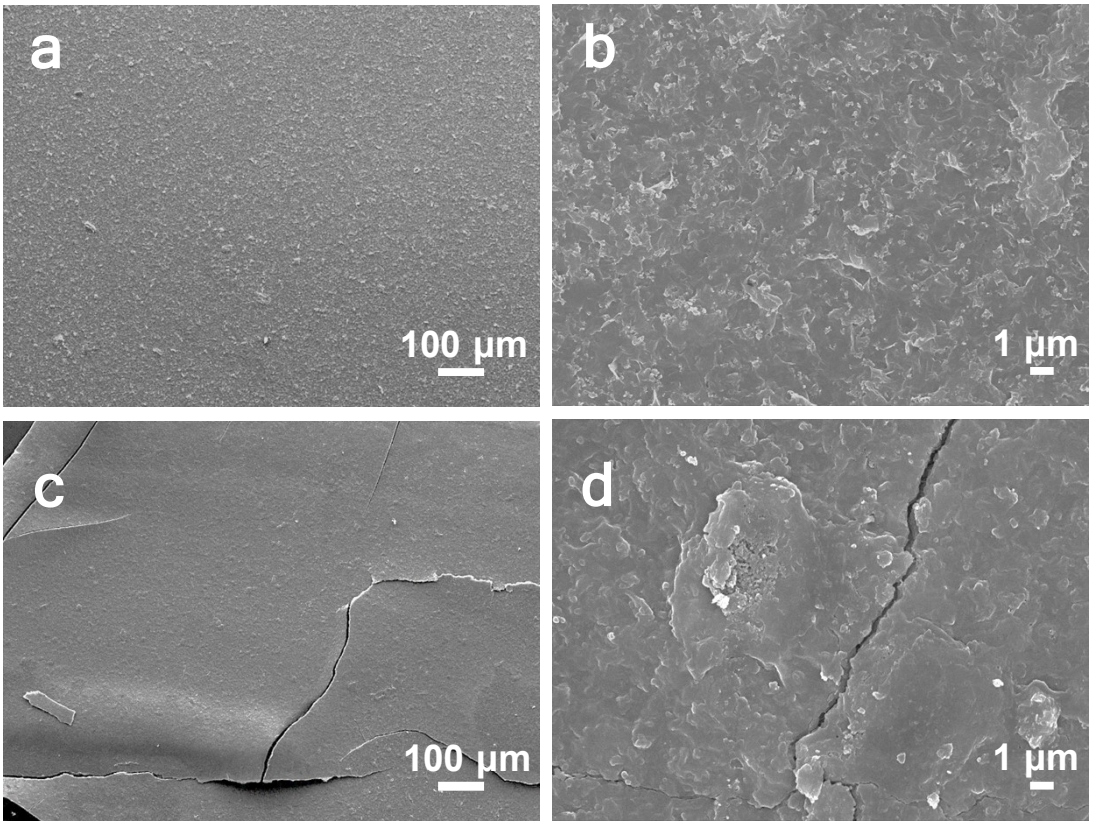

Figure S16 SEM images of the CM modified separator adjacent to the cathode side (a-b) before and (c-d) after 100 cycles.

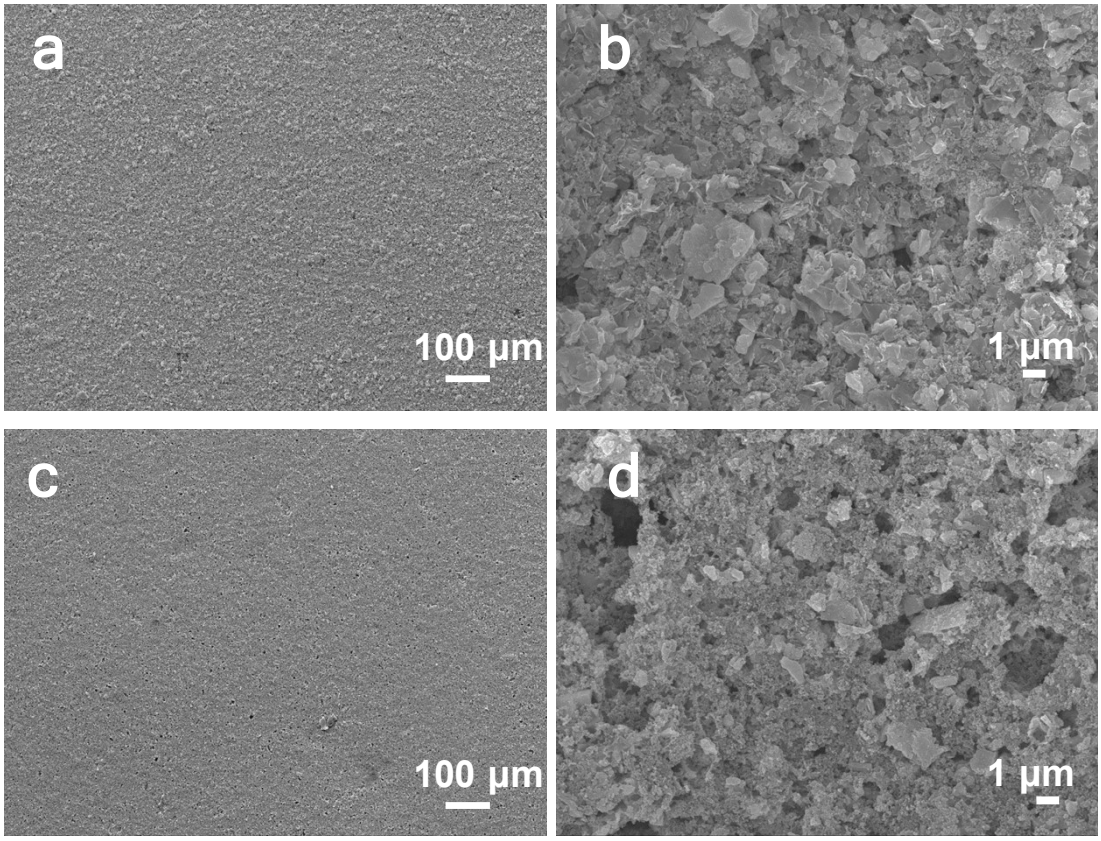

Figure S17 SEM images of the MoS_2 modified separator adjacent to the cathode side (a-b) before and (c-d) after 100 cycles.

Table S1 The measured parameters for the electrolyte permeability of various separators.

Sample	Initial mass (g)	Terminal mass (g)	Time (min)	Pressure (bar)	Permeability (L m^{-2} h^{-1} bar^{-1})
PP separator	16.4567	22.5213	5	7	28.04
CM	16.5625	16.8633	5	7	1.39
MoS_2	16.6041	20.7357	5	7	19.11
CM/MoS_2	16.5933	20.6588	5	7	18.80

Table S2 The fitted resistance parameters of the coin cells with various modified separators.

Sample	R1	R2	R3
CM/MoS_2	1.665	9.058	7.272
MoS_2	2.304	14.01	5.9
CM	1.606	22.4	6.694
PP separator	1.339	20.53	3.36

Table S3 Comparison of various performance parameters with the reported MoS_2 and MXene–based modified interlayers.

Samples	Sulfur loading (mg cm^{-2})	Specific capacities at various C-rates (mAh g^{-1})						Capacity retention (%)	Cycling number
		0.1C	0.2C	0.5C	1C	2C	3C		
Our Work	2	1336	1178	1001	896	810	652	73	500
MoS_2/graphene[6]	1	/	/	1245	1082	/	949	71	500
MXene nonosheets[7]	1.7	/	1062	756	634	517	/	71.48	400
Ti_3C_2 nanoribbon[8]	0.7-1	/	1062	744	691	513	/	50.4	200
MoS_2/TiN[9]	2.5	/	1480	1242	1010	841	697	50	500
Co_9S_8@MoS_2[10]	3	1221	1065	978	806	601	/	63.5	500
MoS_2[11]		1471	1039	770	550	/	/	49.6	600
Porous MXene[12]	0.91	1282	1004	861	740	677	/	72.4	500

References:

1. M.L. Liu, L. Li, M.J. Tang, L. Hong, S.P. Sun and W. Xing, *Chemical Engineering Science*, 2021, **245**, 116854.
2. M.L. Liu, L. Li, Y.X. Sun, Z.J. Fu, X.L. Cao and S.P. Sun, *Journal of Membrane Science*, 2021, **617**, 118644.
3. T.D. Lu, L.L. Zhao, W. F. Yong, Q. Wang, L. Duan and S.P. Sun, *Chemical Engineering Journal*, 2021, **409**, 128206.
4. G. G. Kresse and J. J. Furthmüller, *Physical review. B, Condensed matter*, 1996, **54**, 11169.
5. P. J. P. R. B. Chl, 1994, **50**, 17953-17979.
6. Z. Cheng, Y. Chen, Y. Yang, L. Zhang, H. Pan, X. Fan, S. Xiang and Z. Zhang, *Advanced Energy Materials*, 2021, **11**, 2003718.
7. S. Zhang, N. Zhong, X. Zhou, M. Zhang, X. Huang, X. Yang, R. Meng and X. Liang, *Nano-Micro Letters*, 2020, **12**, 112.
8. Y. Dong, S. Zheng, J. Qin, X. Zhao, H. Shi, X. Wang, J. Chen and Z.-S. Wu, *ACS Nano*, 2018, **12**, 2381-2388.
9. M. Waqas, Y. Han, D. Chen, S. Ali, C. Zhen, C. Feng, B. Yuan, J. Han and W. He, *Energy Storage Materials*, 2020, **27**, 333-341.
10. B. Li, Q. Su, L. Yu, J. Zhang, G. Du, D. Wang, D. Han, M. Zhang, S. Ding and B. Xu, *ACS Nano*, 2020, **14**, 17285-17294.
11. Z. A. Ghazi, X. He, A. M. Khattak, N. A. Khan, B. Liang, A. Iqbal, J. Wang, H. Sin, L. Li and Z. Tang, *Advanced Materials*, 2017, **29**.
12. D. Xiong, S. Huang, D. Fang, D. Yan, G. Li, Y. Yan, S. Chen, Y. Liu, X. Li, Y. Von Lim, Y. Wang, B. Tian, Y. Shi and H. Y. Yang, *Small*, 2021, **17**, 2007442.